CHARACTERISTICS OF RE-LIQUEFIED BEHAVIOR OF SAND BY MEANS OF IMAGE ANALYSIS IN STACKED-RINGS SHEAR APPARATUS

Seto WAHYUDI[1], Junichi KOSEKI[2] and Takeshi SATO[3]

ABSTRACT: This paper is aimed to investigate the effects of pre-liquefaction history on the re-liquefaction characteristics of sand by means of image analysis in a newly developed stacked-rings shear apparatus. The new apparatus enables us to project qualitatively the behaviors of soil during re-liquefaction, while the application of image analysis enables us to investigate in detail the local deformation of re-liquefied soil. The results from this investigation are as follows: 1) The increase of specimen's density in post liquefaction is less important than the effects of pre-shearing history on re-liquefied soil. 2) The pre-shearing history of soil may produce two outcomes. Small amplitude pre-shearing history causes stronger re-liquefaction resistance while large amplitude causes the opposite result. 3) Image analysis results show that large deformation causes larger changes in soil structure, thus their re-liquefaction resistance becomes weaker.

Key words: Pre-shearing, re-liquefaction, stacked-rings shear apparatus, shear strain amplitude, specimen's density, image analysis, local shear strain.

INTRODUCTION

Recently, the re-liquefaction phenomenon has been re-emerged to be one of the major issues since the 2011 Great East Japan Earthquake Disaster. It was reported that liquefaction had re-occurred at 150 sites during the period from year of 745 to 2008 throughout Japan (Wakamatsu, 2000). In addition, another 60 cases of re-liquefaction were also found in the 2011 Earthquake (Wakamatsu, 2012). These evidences raised concern among researchers about the potential danger of re-liquefaction that might occur in the future large earthquake. The types of areas which are prone to liquefy repeatedly are the areas where young sandy soil deposit exists such as the reclaimed land and the areas around downstream of rivers.

Generally, we tend to think that once the soil liquefies, then it may become harder for the same soil to liquefy at another time. Finn et al. (1970) and Seed et al. (1977) were among the first frontier researchers to investigate this issue. They studied the effects of pre-shearing history of soil on the resistance of the next liquefaction. Their early findings showed a disagreement about the impacts of pre-shearing history on the re-liquefaction resistance of soil. Finn et al. (1970) found that the pre-sheared sample should expect an increase of its re-liquefaction resistance while Seed et al. (1977) found the opposite impact of the pre-shearing history on the future liquefaction. Later, further investigation on the effects of pre-shearing history on re-liquefied soil was conducted by Ishihara and Okada (1978), who found that the soil re-liquefaction resistances can increase or decrease depending on whether or not the pre-sheared sample passing the so-called Phase Transformation line. The resistance of future liquefaction was expected to decrease when previous liquefaction passed through the Phase Transformation line while the opposite impact was expected to occur when the pre-sheared sample did not pass the line. Oda et al., (2001) conducted comprehensive investigation on the parameters that might have significant impact in determining the characteristics of re-liquefied soil, including the effects of induced anisotropy, inherent anisotropy, loading direction, and the uniformity of sample among others. Since then, recent study on the re-liquefied soil was done by Yamada et al.

[1](2010). They specifically investigated the effects of soil anisotropy induced by the residual strain in post liquefaction combined with the effects of different loading directions.

The frontier studies that have been discussed earlier were all conducted either by triaxial or hollow cylinder torsional shear apparatus. Both of these typical apparatuses use flexible membrane. Therefore, the number of re-liquefaction stages that can be performed was usually up to two stages. In this study, the investigation of the re-liquefaction characteristics of sand was conducted by using a newly developed machine so-called stacked-rings shear apparatus. Unlike other testing apparatuses, the stacked-rings shear apparatus is capable of maintaining the shape of the specimen to remain constant due to its rigid metal rings boundary. However, the absence of flexible membrane on the stacked-rings shear apparatus has its own drawback as will be discussed later. By taking the advantage of this apparatus, we are able to perform not just a few number of re-liquefaction stages, but virtually unlimited number of liquefaction stages with a single specimen. The test results using the stacked-rings shear apparatus will give us qualitative behavior of the re-liquefied soil. In addition, the application of image analysis would give us clearer insight on the mechanism that takes place in re-liquefied soil.

This paper aims to investigate the effects pre-liquefaction history with different shear strain amplitudes on the behavior of re-liquefied sand by using image analysis.

TEST PROCEDURES

The outline of the newly developed machine so-called stacked-rings shear apparatus is shown in Fig. 1. The axial load is applied to the specimen through a pneumatic system using bellofram cylinder while the torque is controlled by direct motor system. This direct motor system allows the apparatus to apply virtually endless rotation in both clockwise and anti-clockwise directions. Two two-component load cells are installed in this apparatus to measure the axial load and the torque at both the top and bottom positions. In the current setting of the apparatus, the capacities of the load cells for the axial load and torque are 30 kN and 1500 N.m, respectively. The applied axial load and torque to the specimen are controlled solely by the upper load cell while the bottom one measures the transferred loads. Later, the difference of the measured stresses in both load cells will be used to calculate the friction angle between soil and metal rings (δ) mobilized during the test. Need to be mentioned that in the current setting of the apparatus, both lateral and radial stresses (σ_r and σ_θ) cannot be measured. These stresses were evaluated by assuming the coefficient of lateral earth pressure at rest (Ko) is equal to 0.5 (in case of Toyoura sand).

1. Repeated liquefaction test:

In the stacked-ring shear apparatus, an annular specimen is placed in between two parts of stacked-rings, which are inner and outer parts as shown in Fig. 2(a). Each inner and outer part is composed of 11 pieces of vertically-stacked annular rings having a thickness of 5 mm as shown in Fig. 2(b). It needs to be mentioned that there is no direct contact between the rings. Six pieces of metal bearings with a thickness of 0.1 mm were inserted in between the rings, so that friction in the circumferential direction can be reduced as minimum as possible. This 0.1 mm gap between the rings is small enough to ensure the sand particles with a mean diameter larger than 0.1 mm (D_{50}= 0.163mm) will not extrude during shearing. Each ring is allowed to move in circumferential direction, while it is restrained in the vertical direction, which may induce friction in the vertical direction with sand particles. The inner and outer diameters of the specimen are 90 mm and 150 mm, respectively, and the height of the specimen is 55 mm.

Toyoura sand was used as the test material. Its particles have an angular or sub-angular shape with

[1] Graduate Student, Department of Civil Engineering, The University of Tokyo
[2] Professor, Institute of Industrial Science, The University of Tokyo
[3] Technical Director, Integrated Geotechnology Institute Ltd.

the following physical properties: specific gravity, G_s=2.656; mean diameter, D_{50}=0.162mm; fines content, F_c=0.1%; max. void ratio, e_{max}=0.992; min. void ratio, e_{min}=0.632. Specimens were prepared by pluviation of air-dried sand particles into a mold through air. Their falling height was kept constant throughout the pluviation process in order to obtain specimens with highly uniform density. Three specimens having the initial relative density (Dr_0) in the range of 53% - 56% were prepared for this study. Each of the specimens was sheared cyclically while keeping the specimen volume constant until the shear strain double amplitudes ($\gamma_{DA.Max}$) exceed 2.0%, 5.0% and 10.0%, respectively.

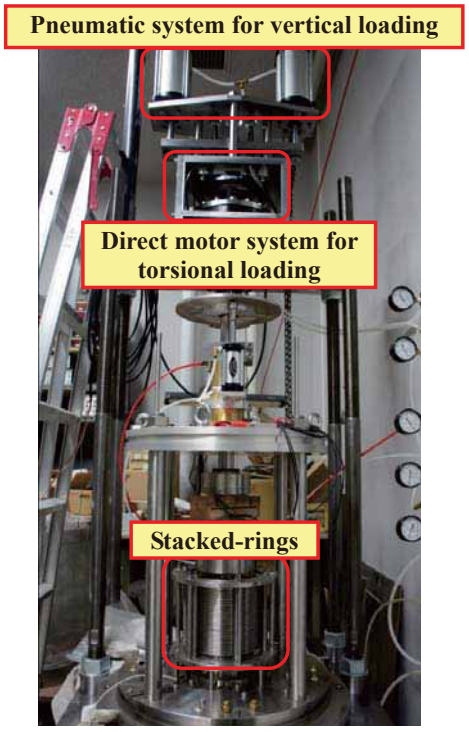

Fig. 1: Stacked-rings shear apparatus

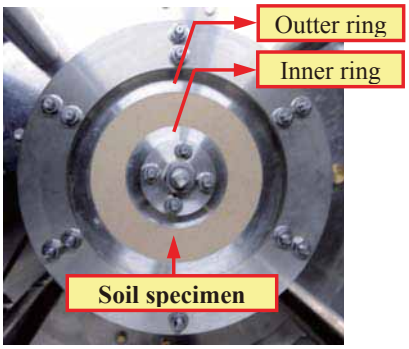

Fig. 2(a): Plan view of stacked-rings

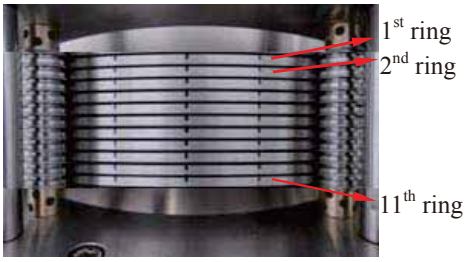

Fig. 2(b): Side view of stacked-rings

Figures 3(a) and Fig. 3(b) show the sequences to conduct a re-liquefaction test in this study. First, prior to the application of cyclic shear loading, each specimen was consolidated one-dimensionally with vertical stress of 5 kPa (state A) up to 200 kPa (state B). Then, the specimen was subjected to the cyclic shear stress of 20 kPa ($\pm\tau$ = 20 kPa) under constant volume condition. The liquefaction was defined as the state whenever the double amplitude of shear strain reached 2.0% ($\gamma_{DA(2.0\%)}$), while the cyclic loading was continued to achieve the pre-fixed $\gamma_{DA.Max}$ value (state C). Then, the stage of liquefaction was completed by adding another half cycle of shear loading from state C to state C', where the shear strain (γ) is equal to zero as shown in Figs. 3(c) and 3(d). States C' and D in this study were set to be the ending and the starting states of each stage during re-liquefaction test, respectively. The reason to end each liquefaction stage at the zero shear strain (γ=0) was to prevent an additional effect of soil anisotropy induced by residual deformation in post liquefaction (Ishihara and Okada, 1978). The next liquefaction stage was started by re-consolidating the liquefied specimen into their original effective vertical stress (σ_v') of 200 kPa at state D. Then, the subsequent liquefaction test was conducted by following the same procedures as the one described in the first liquefaction stage.

On each liquefaction stage, the liquefaction resistance was evaluated by calculating the number of cycles needed to reach the double amplitude of shear strain 2.0%, using the equation shown below.

$$N\gamma_{DA} = \frac{\left(\gamma_{DA} - \gamma_{DA(Ni)}\right)}{\left(\gamma_{DA(Ni+0.5)} - \gamma_{DA(Ni)}\right)} \times 0.5 + Ni$$

where, γ_{DA} is the target shear strain double amplitude, which in this study is 2.0%; $\gamma_{DA(Ni)}$ and $\gamma_{DA(Ni+0.5)}$ are the shear strain double amplitude measured during the loading cycle just before and half cycle after the target of shear strain double amplitude, and Ni is the number of cycle just before the target of shear strain amplitude was reached.

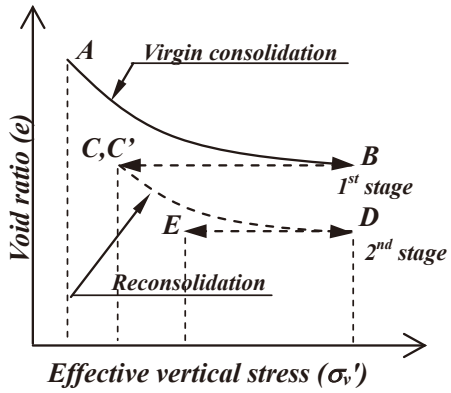

Fig. 3(a): Typical void ratio and vertical stress relationship in re-liquefaction test

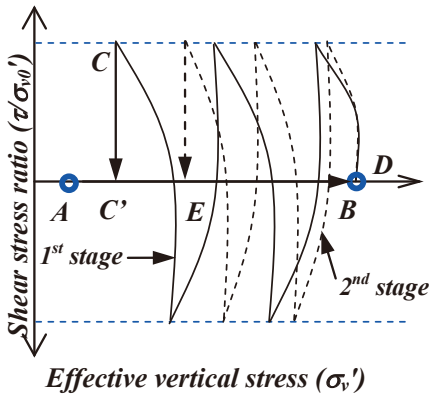

Fig. 3(b): Typical shear stress ratio and vertical stress relationship in re-liquefaction test

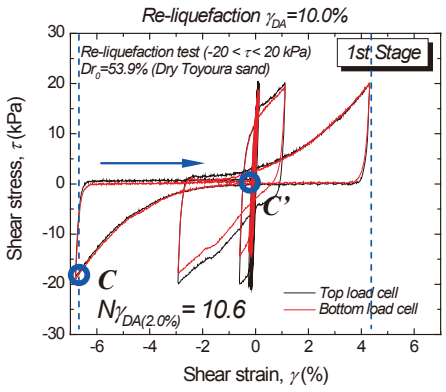

Fig. 3(c): Typical shear stress and shear strain relationship in one stage of re-liquefaction test

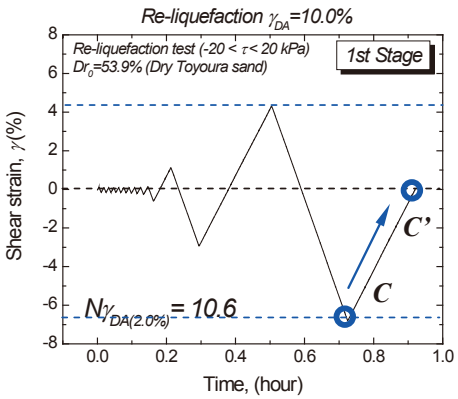

Fig. 3(d): Typical shear strain and time relationship in one stage of re-liquefaction test

Instead of using saturated specimen, dry specimen is used to perform liquefaction test in stacked-rings shear under constant volume condition. It is based on the assumption that the decrease in applied vertical stress (σ_v) during shearing in constant volume test is equal to the increase in shear-induced pore water pressure (u) that would occur in an undrained saturated test. Bjerrum and Landva (1966) proposed this assumption for DSS test (Direct Simple Shear) while Finn and Vaid (1977) confirmed it later for both triaxial and DSS tests.

2. Image analysis:

The configuration setting on the application of image analysis in this experiment is shown in Fig. 4. For this purpose, the outer part of each ring is marked with twelve dots. The distance between each dot is 36.7 mm or equal to every 30° in circumferential angle. During cyclic shear loading, the movement of these dots is captured by a digital camera. The camera is connected to the computer system for the automation purpose during the entire tests. In the current setting, the camera is set to take the picture by the rate of 0.2 min./pic or equal to a shear strain increment of 0.5% /pic.

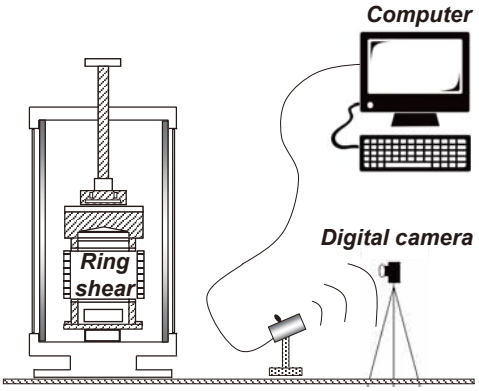

Fig. 4: Configuration of photo control system

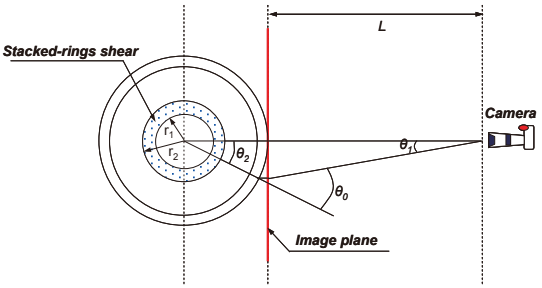

Fig. 5: Plan view of image configuration

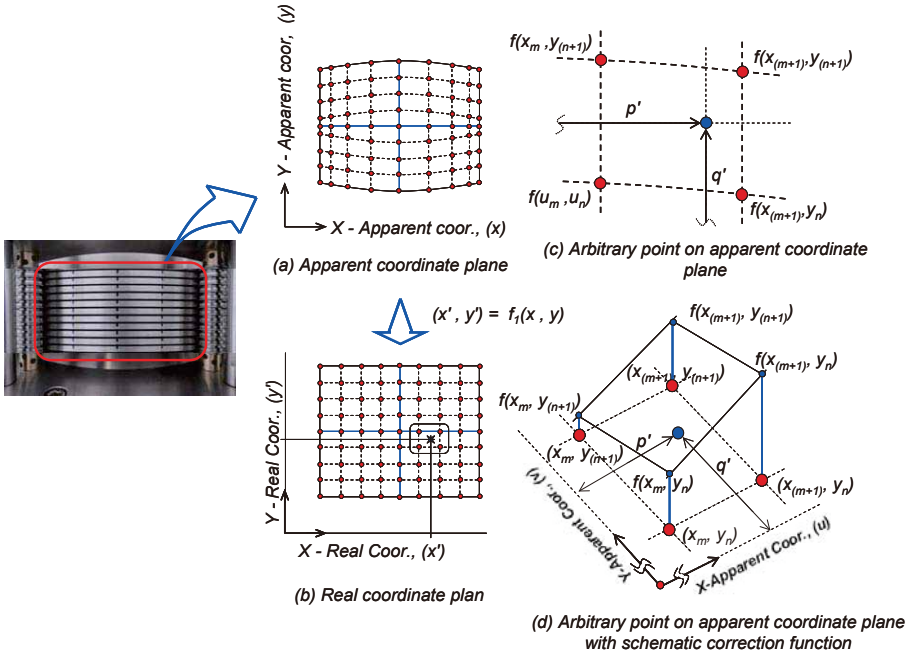

Fig. 6: Image analysis by bilinear interpolation method

As we understand, the camera works by transforming the three-dimensional object into the two-dimensional image as projected on the plane as shown in Fig. 5. Since the shape of the stacked-rings itself is cylindrical, thus the movements of the dot captured by the camera are not the real ones. This distortion is caused by the bending of image due to depth effect. In the imaging research field, this

kind of distortion is called barrel distortion. In addition, unsymmetrical initial setting of the camera could also cause distortion of the image. To solve this problem, a mathematical tool is employed in this paper to convert the apparent/distorted coordinates taken by the camera into their real ones.

In analyzing the image, the apparent orthogonal coordinates (*x,y*) were tracked by Tr-2D imaging software. This software is capable of tracking the movements of each dot with an accuracy of about 0.1 mm. Then, the correction is applied to convert the apparent/distorted coordinates into their real ones (*x',y'*) as shown in Figs. 6. In this study, the correction functions were formulated using a simple polynomial function as shown in Eq. 1 below.

$$(x', y') = f_1(x, y)$$
$$x'_{(m)} = a_{0(m)}.1 + a_{1(m)}.x_{(m)} + a_{2(m)}.y_{(m)} + a_{3(m)}.x^2_{(m)} + a_{4(m)}.x_{(m)}.y_{(m)} + a_{5(m)}.y^2_{(m)} \quad (1)$$
$$y'_{(n)} = b_{0(n)}.1 + b_{1(n)}.x_{(n)} + b_{2(n)}.y_{(n)} + b_{3(n)}.x^2_{(n)} + b_{4(n)}.x_{(n)}.y_{(n)} + b_{5(n)}.y^2_{(n)}$$

where, *x'* and *y'* are the real coordinates in horizontal and vertical directions, respectively; *x* and *y* are the apparent coordinates in horizontal and vertical directions, respectively; the coefficients a_0 through a_5 and b_0 through b_5 are assigned based on calibration results by means of least square error method; *m* and *n* are the number of column and row, respectively.

TEST RESULTS AND DISCUSSIONS

To impart the pre-shearing history into the specimens, each of them was sheared with pre-fixed maximum shear strain double amplitudes ($\gamma_{DA.Max.}$) of 2.0%, 5.0% and 10.0%. Figure 7(a) shows a typical shear stress and shear strain relationship while Fig. 7(b) shows a shear stress and vertical stress relationship for the first stage of re-liquefaction test. It can be noticed in Fig. 7(b) that prior to the application of cyclic shear loading, the vertical stresses between the top ($\sigma_{v.T}$) and the bottom load cells ($\sigma_{v.B}$) started with different initial values. This difference was caused by the friction between the sand particles and metal rings during consolidation/re-consolidation as can be seen clearly in Fig. 8(a). This figure shows typical volume change and vertical stress relationship during consolidation/re-consolidation in a re-liquefaction test. It was found that the friction between soil particles and metal rings generally consumed about 50% - 52.0% of the vertical stress applied to the top of the specimen. Based on that, the friction angle in vertical direction (δ_{hv}) was evaluated. To evaluate the friction angle in circumferential direction (δ_{hh}), the difference of the torque measured at top (τ_{Top}) and bottom load cells (τ_{Bot}) was used for the calculation.

Figure 8(b) shows a typical result of soil-ring's wall friction angle and vertical stress relationship during consolidation/re-consolidation. It was found that typical soil-ring's wall friction angle in both vertical and circumferential directions were about 22° and 1°, respectively. This result shows large friction is generated in the vertical direction while relatively small friction is generated in the circumferential direction. However, these amounts of friction were found to be nearly constant prior to each liquefaction test. Therefore, qualitative observation on the effects of pre-shearing history on the re-liquefied soil still can be made.

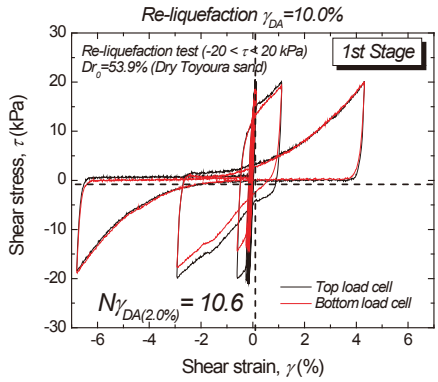

Fig. 7(a): Typical shear stress and shear strain relationship

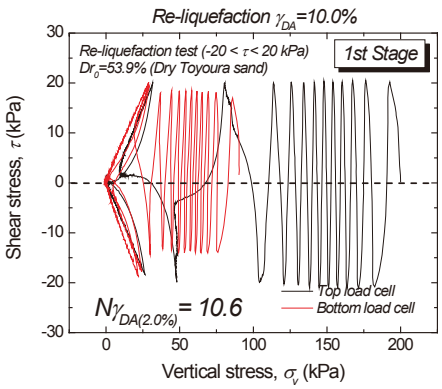

Fig. 7(b): Typical shear stress and vertical stress relationship

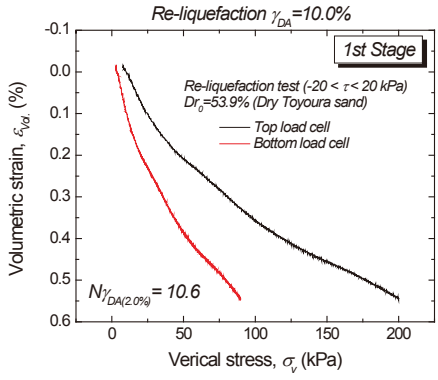

Fig. 8(a): Typical volumetric strain and vertical stress relationship

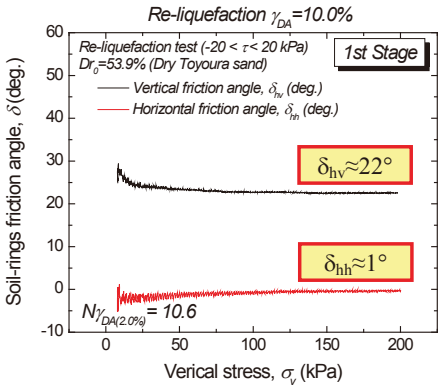

Fig. 8(b): Typical soil-rings friction angle and vertical stress relationship during consolidation

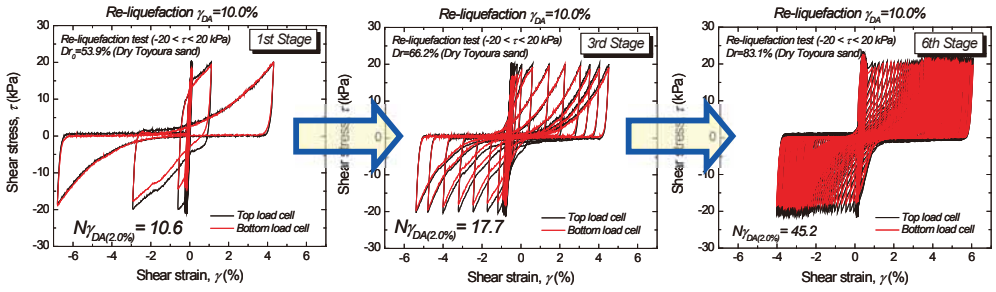

Fig. 9: Number of cycle to liquefy and change in relative density relationship in re-liquefaction test

1. Experimental results

Figure 9 shows typical results of a re-liquefaction test. In each stage, the number of cycle needed to

liquefy and the changes in specimen's density due to re-consolidation were evaluated. Figure 10(a) shows the relationship between the number of cycle to liquefy and the liquefaction stage. From this figure, it can be seen that the specimen sheared with 2.0% shear strain double amplitude showed the most significant increase of its re-liquefaction resistance, then followed by the specimens sheared at 5.0% and 10.0% shear strain double amplitudes subsequently.

Figure 10(b) shows the relationships between the change in specimen's density and the liquefaction stage. This figure shows that the smaller the shear strain applied, the smaller the increase of the specimen's density during re-consolidation. This figure also shows that the specimen's densities increase almost linearly on each stage during re-consolidation in post liquefaction. Interestingly, this figure may suggest that larger increase of the specimen's density did not cause larger increase of their liquefaction resistances. In fact, the current test results showed an opposite trend, in which the larger the shear strain applied, the weaker the soil resistances against re-liquefaction are. This only suggests that other factors play more important role than the increase of specimen's density alone in determining the re-liquefaction resistance of soil.

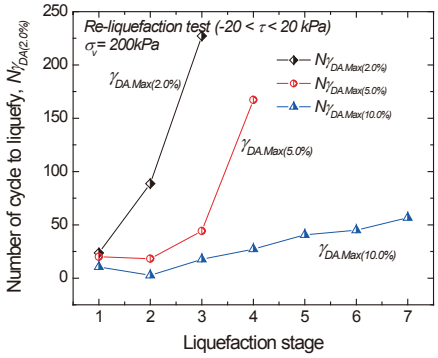

Fig. 10(a): Number of cycle to liquefy and liquefaction stage relationship in re-liquefaction test

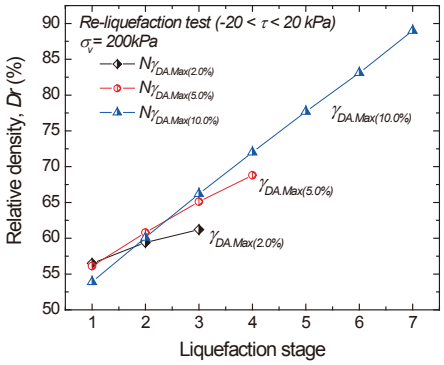

Fig. 10(b): Change in relative density and liquefaction stage relationship in re-liquefaction test

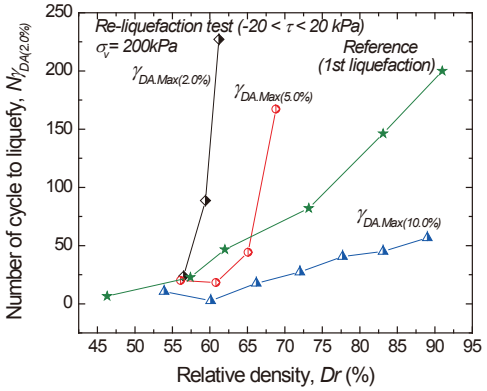

Fig. 10(c): Number of cycle to liquefy and change in relative density relationship in re-liquefaction test

By combining the results shown in Fig. 10(a) and 10(b), the relationship between the number of cycle to liquefy and the change of specimen's density is plotted in Fig. 10(c). In addition, the results of all the re-liquefaction tests were overlapped with a set of virgin liquefaction tests as a reference, which were conducted with various relative densities. These reference soils are the soil sample that liquefied for the first time (single stage liquefaction test).

From this figure, the specimen sheared until 2.0% shear strain double amplitude showed larger re-liquefaction resistances than the reference soils at any re-liquefaction stages. The specimen sheared with 5.0% shear strain double amplitude showed smaller re-liquefaction resistances against the reference soils during several early stages (2^{nd} and 3^{rd} stages). However, as the liquefaction stages continued, the soil resistance increased exponentially and became stronger than the reference ones. In the last test, where the specimen was sheared with 10.0% shear strain double amplitude, the re-liquefaction resistance appeared to be always smaller than the reference soils at any stages. These results clearly suggest a significant impact of the shear strain amplitude of pre-sheared soil in determining their re-liquefaction resistances. The larger the pre-shearing history applied, the smaller the soil resistance against re-liquefaction.

The re-liquefaction resistance on the specimen sheared up to 2.0% shear strain double amplitude ($\gamma_{DA.Max(2.0\%)}$) increased exponentially in its 2^{nd} and 3^{rd} re-liquefaction stages. On the other hand, the re-liquefaction resistance on the specimen sheared up to 10.0% shear strain double amplitude was decreased in the 2^{nd} stage, and then gained minor increase in the following stages. This significant difference shown in both tests is possibly caused by the changes of soil structure as will be discussed later. Small shear strain amplitude of pre-shearing history may only cause re-arrangement of soil structure. In this range of shear strain amplitude, the soil particles experience more contraction than dilation, thus the soil structure becomes stronger in the next liquefaction. In the opposite case, large soil deformation exceeding some limit (threshold) may alter the entire soil structure and even creates damaging impacts to the soil resistance in the future liquefactions. The larger the soil deforms, the greater the changes in soil structure are. Thus, their resistance against re-liquefaction becomes weaker. However, these outputs only show us the global behaviors of the soil and not enough to explain quantitatively the mechanism. Therefore, the observation by image analysis is made in the current study to see more in detail the local behaviors of each section of the specimen.

2. Image analysis results

Each liquefaction stage is intentionally set to start and end at the same origin of $\gamma_{glo.}$= 0%, where $\gamma_{glo.}$ is defined as the global shear strain of the specimen measured at the top cap. Therefore, it is expected that the effect of induced-anisotropy would be negligible. The application of image analysis method in this experiment aims to capture the effects of shear strain amplitudes on the characteristics of re-liquefied soil.

To evaluate the local shear strain of the specimen, the 55 mm-high specimen is divided into 10 sections, where a section of specimen is located in between the center point of two rings as shown in Fig. 2(b). For the simplicity reason, these 10 sections are reduced into 5 sections by averaging the measured values on a neighboring pair of sections. From bottom to up, the 5 sections represent the lowest, middle-lower, center, middle-upper and upper-most sections, subsequently. Figure 11(a) shows the typical local shear strain measurements on 1^{st} liquefaction stage (virgin liquefaction), while Fig. 11(b) shows the results on the 2^{nd} liquefaction stage for the specimen sheared with 5% shear strain double amplitude ($\gamma_{DA.max(5.0\%)}$) test. All the local shear strain (γ_{Loc}) measurements obtained from image analysis were compared with the global one ($\gamma_{glo.}$). From these figures, we can see that the local shear strains matched with the global one when it was sheared up to 1.0% shear strain double amplitude. After that, the local strains at some sections started to deviate from the global one. If we look into the detail, the initial deviation started when the vertical stress reached nearly zero value (σ'_v=0 kPa) for the first time. Then, as the shear loading continued, the deviation became larger-and-larger.

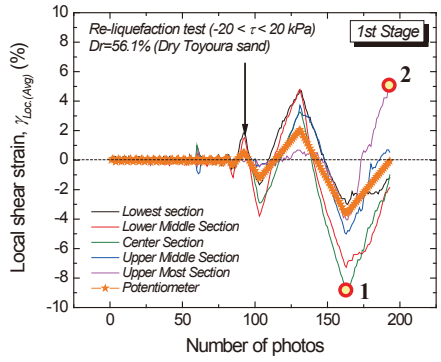

Fig. 11(a): Local shear strain deformation history in the 1st liquefaction on $\gamma_{DA.max(5.0\%)}$ test

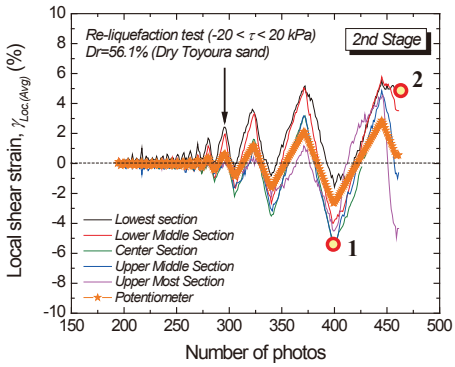

Fig. 11(b): Local shear strain deformation history in the 2nd liquefaction on $\gamma_{DA.max(5.0\%)}$ test

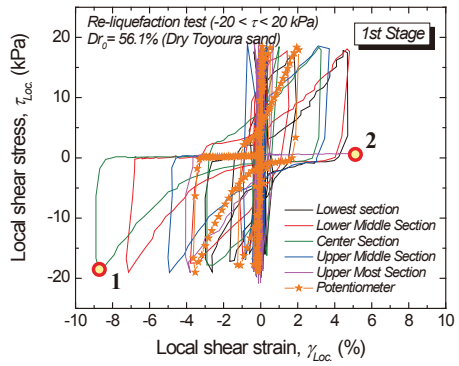

Fig. 12(a): Local shear stress and local shear strain relationship in the 1st stage of $\gamma_{DA.max(5.0\%)}$ test.

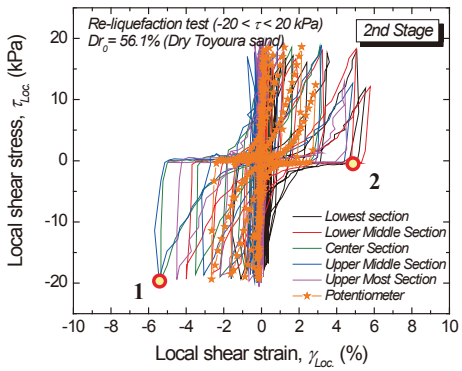

Fig. 12(b): Local shear stress and local shear strain relationship in the 2nd stage of $\gamma_{DA.max(5.0\%)}$ test.

The corresponding typical local shear stress (τ_{Loc}) and local shear strain (γ_{Loc}) relationships for the specimen sheared at 5.0% shear strain double amplitude test are shown in Fig. 12(a) and Fig. 12(b). Need to be mentioned that in the current testing apparatus, both shear stress ($\tau_{\theta v}$) and vertical stress (σ_v) were only measured at the upper-most and lowest sections by the top and bottom load cells, respectively. These stresses at the other sections, which are located in between these sections, were not directly measured. Instead, we assumed that the changes of the shear stresses and vertical stresses from the upper-most to the lowest sections are linear, i.e., the unknown shear stresses and the vertical stresses for the remaining sections were approximated by using linear interpolation.

Points 1 and 2 in Fig. 12(a) and 12(b) mark the maximum local shear strain and residual local shear strain in a re-liquefaction stage, respectively. In this example, the center section has the largest deformation of about 8.7% during 1st liquefaction. However, the upper-most section has the largest residual deformation of about 5.1% at the end of the 1st liquefaction. Similarly, the lower-middle and center sections sheared more then the global one of about 5.4% on the 2nd liquefaction stage, while the lowest section has the largest deformation of about 5.1% at the end of the stage. The summary of the local shear strain on all the three tests will be presented and discussed later.

To summarize the results from the image analysis, we can extract two types of deviations of the

local shear strain, which are the maximum deviation ($\delta_{max.}$) and the residual deviation (δ_{res}). Maximum deviation is the difference between the largest local deformations experienced on each section with respect to the global one. In the similar way, the residual deviation is the difference between the local deformations of each section with respect to the global one at the end of liquefaction stage. The results of maximum deviation and the residual deviation of local shear strain are shown in Fig. 13(a) and 13(b), respectively.

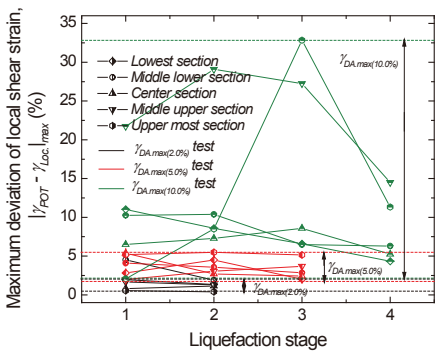

Fig. 13(a): Compilation of max. deviation of local shear strain in all tests.

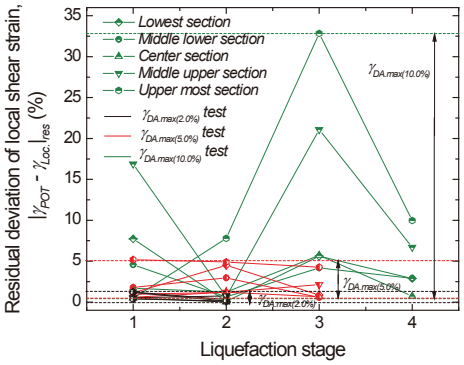

Fig. 13(b): Compilation of end deviation of local shear strain in all tests.

The test sheared with 2.0%, 5.0% and 10.0% maximum shear strain double amplitudes are marked by black, red and green colors, respectively. In addition, the lowest, middle-lower, center, middle-upper and upper most sections in each test is marked with diamond, circle, triangle, reverse-triangle, and hexagonal shapes, respectively.

In Fig. 13(a), we can see clearly that the larger the shear strain applied, the larger the maximum deviation of local shear strain to their global one. The range of maximum deviation in the specimen sheared with 2.0%, 5.0% and 10.0% shear strain double amplitudes are 0.5 - 2.0mm, 1.6 - 5.5mm and 2.1 - 32.8mm, respectively. In the similar way, Fig. 13(b) shows the larger the shear strain applied, the larger the residual deviation at the end of the stage. The range of residual deviation in the specimen sheared with 2.0%, 5.0% and 10.0% shear strain double amplitudes are 0.0 - 1.3mm, 0.5 - 5.2mm and 0.4 - 32.8mm, respectively. These deviations might cause an induced-anisotropy as well as non-uniformity on the liquefied specimen. As reported by Oda et al. (2001) and Yamada et al. (2010), the induced-anisotropy will cause un-equal liquefaction resistance on different loading directions. Though, we expect that the effects of induced-anisotropy would be negligible in these tests for the reason that was mentioned earlier. However, the image analysis results show us that the residual local shear strain on each section may not be zero. This can generate the effect of induced-anisotropy on each section.

In addition to the induced-anisotropy, the deviation of each section also creates the non-uniformity on the re-liquefied specimen. Oda et al (2001) intentionally conducted series of test on the specimen composed by layers of sand with different densities. As expected, the results showed that the non-uniform specimens generally have weaker liquefaction resistances than the uniform one. In the re-liquefaction tests, the sections that were previously sheared larger than others could have looser densities. As a result, these looser layers eventually create the weak layers in the whole specimen that are susceptible to liquefy first in the next liquefaction. As the specimen had been re-consolidated prior to the next liquefaction on every stage, we expect that re-consolidation process may re-arrange the soil particles into more uniform specimen. However, the results show us that even after re-consolidating the specimen, the effects of pre-shearing history on each layer did not vanish.

Both induced-anisotropy and non-uniformity affect the behavior of re-liquefied soil. The larger the degree of these two factors, the weaker the soil's resistance in the future re-liquefaction.

CONCLUSIONS

The investigation on the effects of pre-shearing history in the re-liquefaction behavior of sand revealed several observations, which are:

1. The increase of specimen's density in post liquefaction is less important than the effects of pre-shearing history of soil in determining its re-liquefaction resistance.
2. The pre-shearing history of soil may produce two outcomes. Small amplitude of pre-shearing history causes stronger re-liquefaction resistance while large amplitude causes the opposite result. The reason is due to the changes in soil structure. Small pre-shearing induces the re-arrangement of soil particle, thus soil structure becomes stronger. In the other hand, large deformation at some limit causes large changes in soil structure, thus its resistance against re-liquefaction becomes weaker.
3. Image analysis enables us to look in detail the behavior of each section of the re-liquefied soil. The image analysis results confirm the statement made in point 2. The specimens that were sheared with larger deformation showed larger changes in soil's structure. These changes in soil's structure could possibly generate the induced anisotropy as well as non-uniformity in the liquefied soil, in which the increase of these factors tend to reduce the liquefaction resistance of re-liquefied soils.

REFERENCES

Bjerrum, L. and Landva, A. (1966): "Direct simple shear tests on a Norwegian quick clay." *Geotechnique*, 16(1), pp. 1-20.

Finn, W. D. L., Bransby, P. L., and Pickering, D. J. (1970): "Effects of strain history on liquefaction of sand." *Journal of Soil Mechanic and Foundation, ASCE*, pp. 1917 – 1933.

Finn, W. D. L. and Vaid, Y. P. (1977): "Liquefaction potential from drained constant volume cyclic simple shear test." *Proc. Of the 6th World Conference on Earthquake Engineering, New Delhi, India*

Ishihara, K. and Okada, S. (1982): "Effects of large pre-shearing on cyclic behavior of sand." *Soils and Foundations*, 22(3), pp. 109 – 125.

Oda, M., Kawamoto, K., Suzuki, K., Fujimori, H. and Sato, J. (2001): "Microstructural interpretation on reliquefaction of saturated granular soils under cyclic loding." *Geotechnical and Geo-environmental Engineering*, Vol. 127, no. 5.

Seed, H. B., Mori, K. and Chan, C. K. (1977): "Influence of seismic history on liquefaction sands." *Journal of Geotechnical Engineering Divisions ASCE*, 103, pp. 257 – 270.

Wakamatsu, K. (2000): "Liquefaction history from 416 – 1997 in Japan." *Proc. of 12th WCEE*.

Wakamatsu, K. (2012): "Recurrent liquefaction induced by the 2011 Great East Japan Earthquake compared with the 1987 earthquake." *Proc. of Intl. Symp. on Engineering Lessons Learned from the 2011 Great East Japan Earthquake*, pp. 675 – 686.

Yamada, S., Takamori, T., and Sato, K. (2010): "Effects on reliquefaction resistance produced by changes in anisotropy during liquefaction." *Soils and Foundations*, 50(1), pp. 9-25.